

Partial Knowledge Distillation for Alleviating the Inherent Inter-Class Discrepancy in Federated Learning

Xiaoyu Gan¹, Jingbo Jiang², Jingyang Zhu³, Xiaomeng Wang², Xizi Chen¹, Chi-Ying Tsui²

¹ College of Informatics, Huazhong Agricultural University

² Department of Electronic and Computer Engineering, The Hong Kong University of Science and Technology

³ NVIDIA Corporation

Abstract

Substantial efforts have been devoted to alleviating the impact of the long-tailed class distribution in federated learning. In this work, we observe an interesting phenomenon that certain weak classes consistently exist even for class-balanced learning. These weak classes, different from the minority classes in the previous works, are inherent to data and remain fairly consistent for various network structures, learning paradigms, and data partitioning methods. The inherent inter-class accuracy discrepancy can reach over 36.9% for federated learning on the FashionMNIST and CIFAR-10 datasets, even when the class distribution is balanced both globally and locally. In this study, we empirically analyze the potential reason for this phenomenon. Furthermore, a partial knowledge distillation (PKD) method is proposed to improve the model’s classification accuracy for weak classes. In this approach, knowledge transfer is initiated upon the occurrence of specific misclassifications within certain weak classes. Experimental results show that the accuracy of weak classes can be improved by 10.7%, reducing the inherent inter-class discrepancy effectively.

Keywords

Deep neural networks, federated learning, class imbalance, weak classes

1 Introduction

Federated learning (FL) is a decentralized machine learning paradigm where multiple clients collaborate to train a global model without directly sharing their local data [19]. This approach preserves data privacy by retaining the data on local devices. However, a big challenge to FL is the varying performance across different classes due to the presence of unbalanced sample sizes [31]. When the number of samples for different classes varies substantially, the global model often exhibits bias towards the majority classes, known as ‘head classes’. The minority classes, referred to as ‘tail classes’, become underrepresented [32], thus leading to lower classification accuracy as depicted in Fig. 1(a). However, in this work, we show that ‘dominant’ and ‘weak’ classes consistently exist even when sample sizes are equalized and samples from each class are uniformly distributed across the clients (i.e., with a balanced class distribution both globally and locally). Unlike the minority classes discussed in prior studies, these weak classes are intrinsic to the data itself, rather than being dictated by sample size. The resulting inter-class accuracy discrepancy (ICD) is illustrated in Fig. 1(b).

Fig. 2 presents the class-wise accuracy across several widely used benchmarks in the domain of FL. Each experiment is repeated five times, and the average result is presented. The ICD phenomenon identified in this study exhibits the following characteristics.

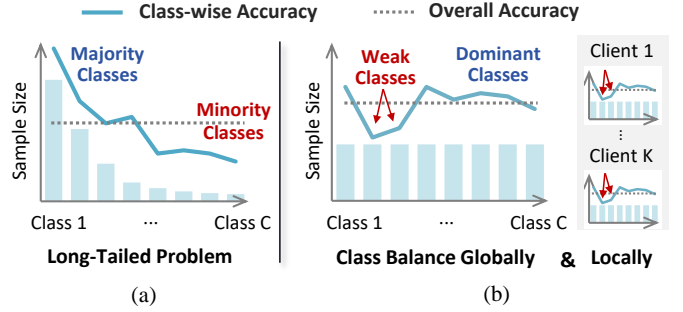


Figure 1: (a) The Conventional Long-tailed Problem; (b) Inherent Inter-class Discrepancies Observed under Balanced Class Distributions (both Globally and Locally).

1) This phenomenon is universally present across different *learning paradigms* and is particularly pronounced in FL compared to centralized learning. 2) Neural networks trained on the same dataset tend to exhibit a very similar ICD, indicating that this phenomenon is irrelevant to the *network structure*. 3) This phenomenon persists no matter whether the *local class distributions* in FL is balanced or not. Notably, as local imbalance intensifies, particularly when samples from weak classes are concentrated within a limited number of clients, the inherent ICD becomes significantly exacerbated. Details will be elaborated upon in the subsequent sections.

Although promising progress has been made in alleviating the inter-class discrepancy brought by class imbalance [32], these techniques cannot be directly applied to the inherent ICD problem. Specifically, current approaches usually focus on rebalancing class distributions by employing techniques such as over-sampling [7] or data augmentation [18] for the minority classes. However, considering that the inherent ICD is not associated with the quantity of samples, these methods may not be sufficient to mitigate the problem effectively.

Experiments indicate that a likely reason for this ICD phenomenon is the intrinsic similarities in high-level features between specific classes. This similarity poses a challenge for the classifier in accurately distinguishing data samples across these classes. In this work, we propose a **federated partial knowledge distillation** (PKD) method to improve classification accuracy for weak classes. Our method is inspired by the observation that an expert trained specifically on a group of confounding weak classes show greater proficiency in differentiating among them. This specialized model focuses solely on extracting and distinguishing the subtle feature differences among these classes and thus yields better accuracy than the model trained jointly on all classes. The term ‘**partial**’

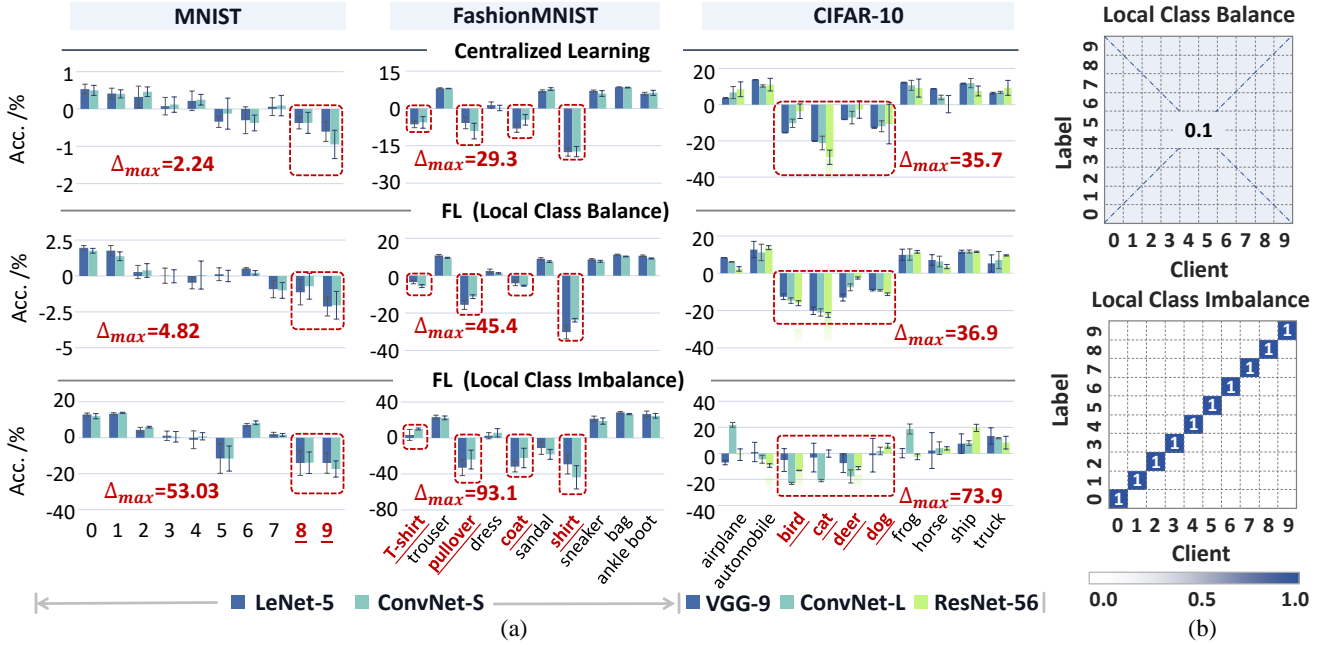


Figure 2: (a) The Class-wise Accuracy (with Mean Subtraction) Based on Different Learning Paradigms and Network Structures (Δ_{max} Refers to the Maximum Discrepancy after a Training Session; the Network Structures, such as VGG-9 [25, 26] and ConvNets [19], are Detailed in Section 4.1.) (b) Sample Distribution in Different Scenarios (Assuming a Total of 10 Clients).

in PKD is shown in several aspects: 1) An expert’s knowledge is confined to specific classes. It is tailored to identify a subset of data that shares analogous high-level features. 2) Knowledge distillation (KD) is triggered only when misclassifications between certain classes happens. Therefore, only a subset of the misclassified samples from these weak classes is considered in computing the KD loss during the training phase. 3) While there might be multiple experts, only up to one expert can be involved in the KD process for any given misclassified sample. Experimental results demonstrate that the proposed PKD method can effectively alleviate the inherent ICD issue by enhancing the classification accuracy of the worst performing classes. In summary, this work makes the following contributions:

- We highlight an interesting phenomenon that certain weak classes are always present, even in ideal scenarios where class distributions are balanced at both the global and local levels. This inherent variance in accuracy across different classes is especially pronounced in the context of FL, reaching up to 45.4% on the FashionMNIST dataset [28] and 36.9% on the CIFAR-10 dataset [12], respectively.
- A federated partial KD method is proposed to enhance the learning process for weak classes. This approach selectively transfers knowledge from class-specific experts to the global student model, all within the FL framework.
- Experimental results show that the proposed method can effectively improve the classification accuracy of the weak classes by over 10.7% and 6.3% on FashionMNIST and CIFAR-10, respectively.

2 Inter-Class Accuracy Discrepancy

2.1 Discrepancy Induced by the Class Imbalance Problem

ICD due to class imbalance. A primary reason for the variance in class-wise accuracy in deep learning is the imbalanced class distribution [1, 8]. The unbalanced sample sizes lead to a dual-fold challenge: 1) Models tend to be biased towards the majority classes, leaving the minority classes under-represented. 2) The lack of data for minority classes makes it even harder to learn the characteristics of these classes [32]. In federated learning, the potential causes for ICD become more complex. The presence of class imbalance at either the global level or within the local dataset of individual clients may diminish the model’s quality. Besides, the mismatch in class distributions between the cloud and the clients may also degrade the performance of the global model [31].

Existing approaches. Existing solutions can be broadly classified into several categories. 1) *Class re-balancing techniques*: These methods focus on offsetting the negative impact of uneven class distribution in training samples. This can be achieved by either over-sampling the minority classes to ensure a more equitable presence in the training data [7, 17], or by re-weighting the training loss values to mitigate the influence of uneven positive gradients [5, 16]. 2) *Data augmentation techniques*: These methods seek to enlarge the sample size or enhance the sample quality of minority classes through data augmentation techniques [3, 11, 24]. Compared to mere re-balancing methods, this approach can potentially enrich the diversity within the minority classes, thereby reducing the risk

of overfitting. 3) Other methods include meta-learning [22], ensemble learning [4, 27], transfer learning [27], and so on. Although significant progress has been achieved in reducing the ICD induced by class imbalance, such strategies may not be directly applicable to addressing the inherent ICD problem, as we will discuss below.

2.2 The Inherent ICD in This Work

Differences from the class imbalance problem. While the weak classes show similar poor accuracy to the minority classes in the class imbalance problem, their underlying causes and potential solutions are distinct. First, the inherent ICD is not a result of uneven sample sizes across different classes. Weak classes consistently exist even in the ideal case where both global and local data are class balanced. Consequently, previous methods that rely on re-sampling local data [24] or clients [33] based on their sample sizes are not feasible in this context. Second, in contrast to minority classes, weak classes are not characterized by data scarcity or a lack of diversity. Experimental results suggest that the conventional data augmentation techniques [6] fail to address the inherent ICD effectively, and in some cases, they might even intensify the inherent accuracy discrepancy.

The inherent ICD phenomenon. Fig. 2(a) shows the class-wise accuracy achieved on three datasets. In each scenario, the total number of samples for each class is kept identical, ensuring that global class balance is maintained. We adopt several commonly used convolutional neural networks and train the models following different learning paradigms. Two local data partitioning strategies are adopted in FL for each dataset, as illustrated in Fig. 2(b). Our results indicate that this inherent ICD is a common phenomenon across various network structures, learning paradigms, and local data partitioning strategies. Most of the dominant classes and the weak classes, e.g., $\{0\}$, $\{1\}$ and $\{8\}$, $\{9\}$ in MNIST [13], remain fairly consistent across various settings. The inter-class accuracy discrepancy is less marked for centralized learning and thus may go unnoticed. However, when it comes to FL, the discrepancy may increase significantly, e.g., reaching up to 45.4% for FashionMNIST. We also test the local class imbalance scenario using a pathological data partitioning strategy proposed in [19]. Specifically, each client is assigned samples from a single class to ensure a clear and straightforward comparison of the class-wise accuracy. As shown in Fig. 2(a), the same group of weak classes is observed, with the accuracy discrepancy further increasing to a significant 53.0% on the MNIST dataset. For more complex datasets like FashionMNIST and CIFAR-10, such discrepancy can reach up to over 73.9%. When evaluated under FL, CIFAR-10 exhibits a reduced discrepancy (Δ) compared to FashionMNIST. This can be attributed to the degradation in overall model performance. For instance, under the extreme local class imbalance scenario, the average accuracy of VGG-9 [25, 26] and ResNet-56 [9] notably drops below 20% on CIFAR-10.

Fig. 3 shows the maximum and minimum class-wise accuracy at each round. While the overall accuracy rises smoothly over time, the difference between the maximum and minimum values continues to be evident. With a balanced class distribution globally and locally, the accuracy discrepancy on the FashionMNIST dataset is 28.9% when there are 10 clients. This value increases significantly

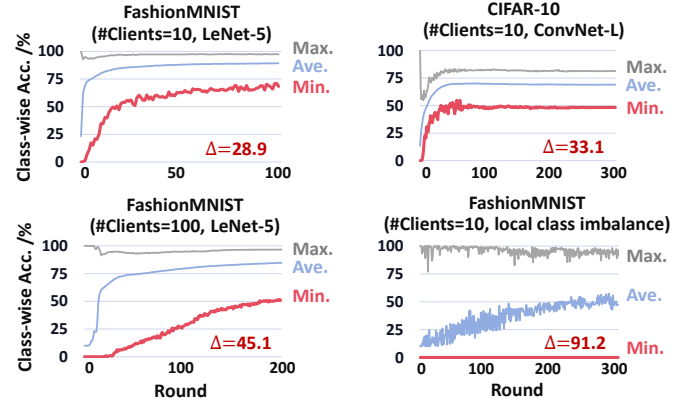


Figure 3: The Maximum, Average, and Minimum Class-wise Accuracy During Training.

as the number of clients grows to 100. In scenarios with local class imbalance, samples from weak classes are concentrated within a small subset of clients, thereby increasing the accuracy discrepancy to 91.2%. The minimum class-wise accuracy is close to zero, indicating that the final model might completely fail in specific classes.

Potential reasons for inherent ICD. Fig. 4 (c) maps the predictions to the original classes to which the data belongs (the models are trained once). It shows that the negative samples of a weak class are often assigned certain wrong labels. For the FashionMNIST dataset with a balanced local class distribution, 62% ($= \frac{85}{137}$) of the misclassified ‘T-shirt’ samples are identified as ‘shirts’ using the LeNet-5 model [13]. Conversely, around 42% ($= \frac{132}{316}$) of the misclassified ‘shirt’ samples are labeled as ‘T-shirts’. Another group of classes that can easily be confused with each other include {‘pullover’, ‘coat’, and ‘shirt’}. For instance, 23% of the misclassified ‘shirt’ samples are identified as ‘pullovers’, while 23% are mistaken for ‘coats’. That is to say, a total of 88% of the misclassified ‘shirt’ samples are incorrectly categorized as other weak classes. This phenomenon becomes particularly pronounced in scenarios with local class imbalance. Approximately 81% of the overall samples categorized under ‘pullover’ and ‘coat’ are misidentified as ‘shirt’ by the LeNet-5 model. A similar phenomenon is observed with other network models, as shown in Fig. 4 (c).

Fig. 4(a) presents some misclassified samples from the two weak class groups, i.e., {‘T-shirt’, ‘shirt’} and {‘pullover’, ‘coat’, ‘shirt’}. It can be seen that these samples exhibit considerable similarities. Fig. 4(a) assesses the similarities in the high-level features (f) between each pair of classes. The weak classes within the two aforementioned groups exhibit a lower Euclidean distance compared to the others, indicating a higher degree of similarity. Therefore, it is challenging for the classifier to differentiate among these classes, leading to lower accuracy and reduced confidence in the model’s predictions. The probability distributions determined by the softmax function are depicted in Fig. 4(b). The figure displays the average probability distribution across all samples within each class. The t-SNE visualizations of feature vectors are presented in Fig. 5.

We further investigate how the classification accuracy for weak classes changes during training. As depicted in Fig. 6, the variance

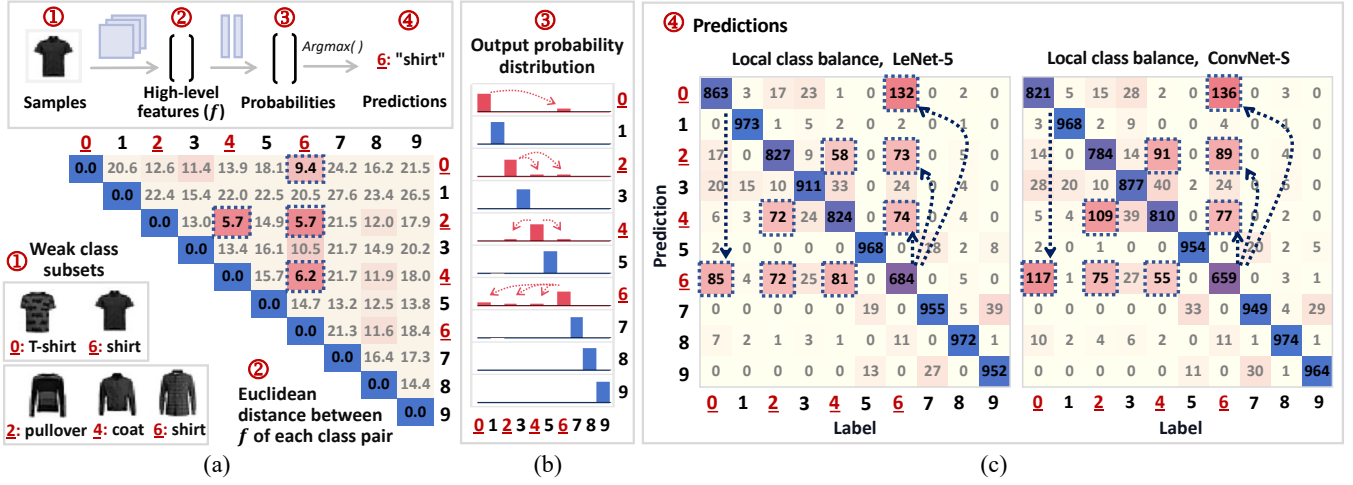


Figure 4: FashionMNIST: (a) Raw Samples and the Similarities in High-Level Features between each Pair of Classes; (b) Output Probabilities (Averaged over 1000 Samples per Class); (c) Prediction Results. For Simplicity, each Class is Assigned a Serial Number. (0: T-shirt, 1: Trouser, 2: Pullover, 3: Dress, 4: Coat, 5: Sandal, 6: Shirt, 7: Sneaker, 8: Bag, 9: Ankle Boot.)

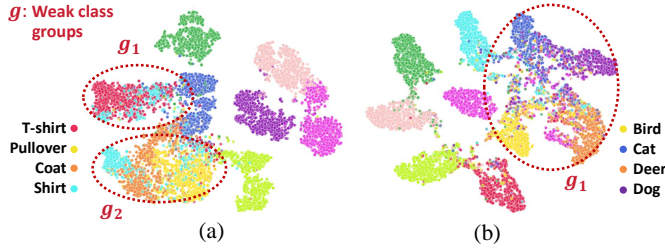


Figure 5: t-SNE Visualizations of Feature Vectors on (a) FashionMNIST and (b) CIFAR-10 (under Local Class-Balanced Scenario, 10 clients).

between two consecutive rounds can reach up to 80% under the local class-imbalanced scenario, even when the global accuracy has become relatively stable. Furthermore, observations reveal a general trend within the group {‘pullover’, ‘coat’, ‘shirt’}: an improvement in the accuracy of one class is accompanied by a corresponding decrease in another’s. The collective accuracy across these three classes appears to be relatively stable. The value hovers around 1/3, implying that the model can generally differentiate weak classes from dominant classes but may fail to recognize the differences among the weak classes themselves.

While FashionMNIST is used as an example for ease of illustration, similar phenomena are observed in other datasets as well. For instance, in the MNIST dataset, samples from the weak classes ‘8’ and ‘9’ are more likely to be misclassified as {‘3’, ‘5’} and {‘4’, ‘7’}, respectively. In the CIFAR-10 dataset, the four weak classes {‘bird’, ‘cat’, ‘deer’, ‘dog’} are prone to confusion with one another. Interestingly, while these classes may not appear similar in their raw image forms, they exhibit similar high-level features that can make them challenging to distinguish for classifiers.

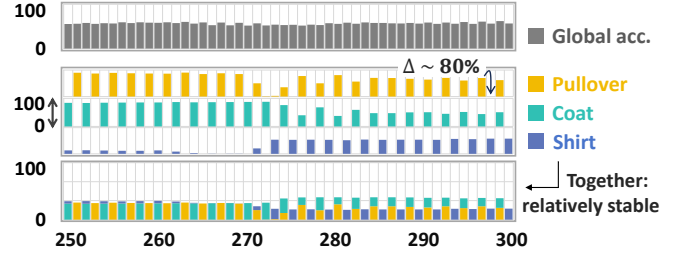


Figure 6: The Class-wise Accuracy (%) During Training (FashionMNIST, under Local Class-Imbalanced Scenario). X Axis: Rounds; Y Axis: Accuracy.

3 The Proposed Algorithm

3.1 Overview

In this work, we introduce a federated partial knowledge distillation (PKD) method to mitigate the impact of inherent ICD and enhance the classification accuracy of weak classes. The flow of the proposed method is outlined in Algorithm 1. The initial model first undergoes several rounds (e.g., 10 to 20) of federated learning. After the warmup stage, it enters an expert learning phase (Line 6). Weak classes are first identified at the edge by examining the output probability distribution obtained from a feedforward pass on the local training set. For illustrative purposes, we use the FashionMNIST dataset as an example. Fig. 7(a) shows the predicted probabilities for classes other than the true class. Each curve represents the probability of samples from one class being misclassified as another class. As depicted in the figure, after the short warmup phase, the chance of misclassifying one weak class as another within the same group—such as a ‘T-shirt’ being predicted as a ‘shirt’ or vice versa—is significantly higher compared to other cases. This distinction can help to identify the weak class groups. Specifically,

Algorithm 1: Overview of the Proposed Method

Input: Number of Rounds (T_1, T_2, T_3); Training Set (D)
Output: Global Model (w)

```

1 Initialize  $w$ ;
2 Stage 1: Warmup
3 for  $i \leftarrow 1$  to  $T_1$  do
4    $w \leftarrow \text{FL}(w, D)$ ;
5 end
6 Stage 2: Expert Learning
7  $g_1, g_2 \leftarrow \text{identify-weak-class}(w, D)$ ; // illustrated in Fig. 7
8  $\text{exp}_1, \text{exp}_2 \leftarrow \text{create-expert}(g_1, g_2)$ ;
9 for  $i \leftarrow 1$  to  $T_2$  do
10    $\text{exp}_1 \leftarrow \text{FL}(D_{g_1})$ ,  $\text{exp}_2 \leftarrow \text{FL}(D_{g_2})$ ; //  $D_{g_i}$ : samples from  $g_i$ 
11 end
12 Stage 3: FL with KD
13 for  $i \leftarrow 1$  to  $T_3$  do
14    $w \leftarrow \text{FL-with-PKD}(w, \text{exp}_1, \text{exp}_2, D)$ ; // Sec. 3.2
15 end

```

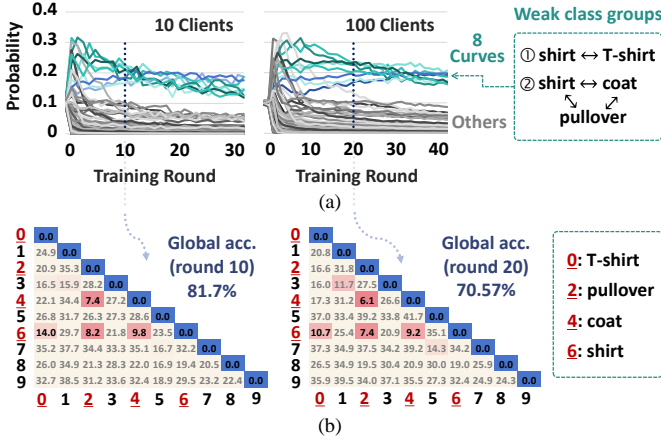


Figure 7: (a) The Probability of Samples from One Class Being Misclassified as Another (FashionMNIST, 10×9 Curves in Total). (b) Euclidean Distance between High-Level Features (f) of each Class Pair at Round 10~20.

the eight highlighted curves in Fig. 7(a) correspond to four pairs of weak classes, namely {'shirt', 'T-shirt'}, {'shirt', 'coat'}, {'shirt', 'pullover'}, and {'coat', 'pullover'}. These four weak class pairs form two groups, as shown in the figure. Fig. 7(b) further presents the similarities in high-level features (f) between each pair of classes at training round 10~20. It is worth noting that both Fig. 7(a) and (b) reveal pronounced disparities between weak classes and others, even during the early training phase.

The identified weak class groups are denoted as g_i in Line 7. For example, in FashionMNIST, g_1 consists of {'T-shirt', 'shirt'}, and g_2 comprises of {'pullover', 'coat', and 'shirt'}. In the case of CIFAR-10, there is only one weak class group {'bird', 'cat', 'deer' and 'dog'}. Once a group of weak classes is identified (g_i), a specialized expert model is trained on a subset of the training data (D_{g_i}) to extract and discern the subtle feature differences among them. (D_{g_i} in

Algorithm 2: FL with Partial KD

Input: Global model (w); Experts (exp_s); Training set (D);
of rounds (T_3); # of clients each round (K);
of local epochs (E); Batch size (B); Learning rate (η)
Output: Global model (w)

```

1 Server Executes
2 for  $t \leftarrow 1$  to  $T_3$  do
3    $S_t \leftarrow \text{random-select-clients}(K)$ ;
4   for each client  $k \in S_t$  in parallel do
5      $w_{t+1}^k \leftarrow \text{client-update}(k, w_t)$ ;
6   end
7    $w_{t+1} \leftarrow \text{aggregate}(w_{t+1}^1, \dots, w_{t+1}^K)$ ;
8 end
9 Client Update // Run on client  $k$ 
10 for each local epoch  $e \leftarrow 1$  to  $E$  do
11    $\mathcal{B} \leftarrow \text{split-into-batches}(D_k, B)$ ;
12   for batch  $\{x, \text{labels}\} \in \mathcal{B}$  do
13      $\text{preds} \leftarrow \text{forward}(w^k, x)$ ;
14      $\text{exp}, \text{sample\_id} \leftarrow \text{activate-expert}(\text{preds}, \text{labels})$ ;
15      $L_{PKD} \leftarrow 0$ ;
16     if  $\text{exp} \neq \text{None}$  then
17        $p_e \leftarrow \text{forward}(\text{exp}, x[\text{sample\_id}])$ ; // Fig. 8
18        $p_s \leftarrow \text{select}(\text{preds}[\text{sample\_id}])$ ; // Fig. 8
19        $L_{PKD} \leftarrow \text{KL-loss}(p_s, p_e)$ ;
20     end
21      $L_{CE} \leftarrow \text{CE-loss}(\text{preds}, \text{labels})$ ;
22      $L \leftarrow L_{CE} + \lambda L_{PKD}$ ;
23      $w^k \leftarrow w^k - \eta \Delta L$ ;
24   end
25 end
26 return  $w^k$  to server;

```

Line 10 refers to the samples from class group g_i .) For simplicity, the expert model adopts the same network structure as the global model, with the exception of the last layer. The last layer has fewer neurons, as the expert is trained for specific classes. All experts are trained within the FL framework, ensuring that no data is uploaded to the cloud. This process takes 25 local training rounds for the FashionMNIST dataset. The overhead of expert training for various benchmarks is analyzed in Section 3.3 and Section 4.5. Typically, one or two experts are adequate to effectively improve the accuracy of the worst-performing classes and alleviate the inherent ICD problem.

In the third stage, partial KD is implemented to transfer the class-specific knowledge from the specialized expert models to the student model, all within the FL framework. This approach is different from the conventional KD methods in several aspects. First, it is triggered only when misclassifications between certain classes (within g_i) happens, which means only a subset of misclassified samples is considered in computing the KD loss. Second, while there may be multiple experts, only one expert can be involved in the KD process for any given misclassified sample. Further details regarding the partial KD process will be presented in the following subsection.

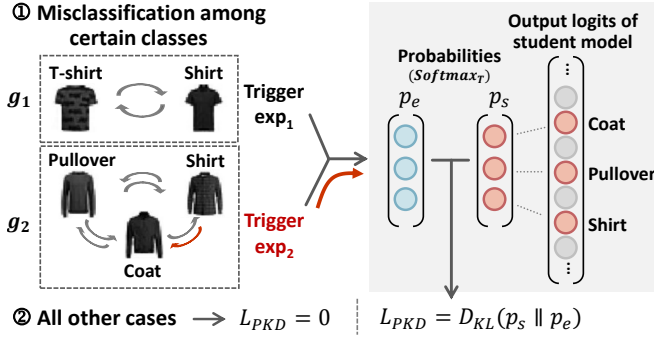


Figure 8: An Illustration Example for the Partial KD Process.

3.2 Partial Knowledge Distillation

The complete pseudo-code of the PKD process is given in Algorithm 2. The overall framework is similar to the standard baseline, FedAvg [19], with the exception of the loss calculation described in Line 22. At each round, the global model is broadcast to K randomly selected clients. Each client trains the model locally for E epochs using its own dataset (Line 5). Then, the local models are sent back and aggregated on the server (Line 7) as described in [19].

During the local training phase on client k , the prediction results ($preds$) are analyzed to detect any instances of misclassification among certain classes in Line 14. The indices of these misclassified samples are denoted as $sample_id$. An illustration example is presented in Fig. 8. Once misclassification within group g_i occurs, the corresponding expert model exp_i is triggered. The experts' prediction results on the misclassified samples ($x[sample_id]$) are denoted as p_e (Line 17). A PKD loss is then computed using the KL divergence [10] between p_s and p_e in Line 19:

$$L_{PKD} = D_{KL}(p_s \parallel p_e) \quad (1)$$

where p_s represents the corresponding predicted probabilities obtained from the student model, as illustrated in Fig. 8. The probabilities p_e and p_s are calculated using the Softmax function with a temperature parameter T , formulated as follows:

$$p_i = \frac{e^{z_i/T}}{\sum_j e^{z_j/T}} \quad (2)$$

where z_i denotes the output logit. Since the PKD method targets specific classes, p_s and p_e only involve a subset of classes, e.g., 3 classes in Fig. 8. In the case where no expert model is activated ($exp = \text{None}$ in Line 16), L_{PKD} is simply set to zero. The complete loss function is formulated as Line 22 in Algorithm 2, where L_{CE} denotes the standard cross-entropy loss, and λ is a hyperparameter.

3.3 Overhead Analysis

While the proposed method can effectively improve the model's performance for weak classes, extra computational costs may be introduced by the expert training in stage 2 and the partial KD process in stage 3. Assuming the computational effort required for a local training round in the baseline scenario is denoted as U . The value can be calculated as follows:

$$U = E \cdot N \cdot (U_{FP} + U_{BP}) \quad (3)$$

where E and N denote the number of local epochs and the total number of samples across all C classes, respectively. U_{FP} and U_{BP} correspond to the computational loads for a forward pass and a backward pass, respectively. The number of computations per round for the proposed method is analyzed in detail as follows.

Stage 1: Warmup

$$U_{T_1} = U \quad (4)$$

Stage 2: Expert learning

$$U_{T_2} = E_{exp} \cdot \sum_i n_{g_i} \cdot (U_{FP} + U_{BP}) = \frac{E_{exp}}{E} \cdot \frac{\sum_i n_{g_i}}{N} \cdot U \quad (5)$$

Stage 3: FL with PKD

$$U_{T_3} = U + n_{KD}^t \cdot U_{FP} \approx (1 + \frac{1}{3} \cdot \frac{n_{KD}^t}{E \cdot N}) \cdot U \quad (6)$$

where E_{exp} denotes the number of local epochs for expert training (usually equal to E), and n_{g_i} represents the number of samples belonging to the class group g_i . The value of $\sum_i n_{g_i}$ ranges from $0.09N$ to $0.6N$ for the datasets used in this work. n_{KD}^t in Eq. 6 denotes the number of misclassified samples that activate the experts in round t . $\frac{n_{KD}^t}{E \cdot N}$ turns out to be a small value ranging from 0.003 to 0.16, indicating that the expert models are only partially involved in the FL process. Compared to the conventional KD methods [21, 29], the overall computational overhead of the proposed PKD method is significantly reduced. This reduction is attributed to the limited number of samples that participate in expert learning and the PKD process. We will further demonstrate that with the same computation cost, the proposed method can achieve higher accuracy than the baseline method.

4 Experimental Results

4.1 Experimental Setups

Datasets. We evaluate the proposed method on several widely-used datasets in FL, including the simple datasets MNIST and FashionMNIST, as well as the more complex datasets CIFAR-10 and CIFAR-100 [12]. We also adopt the more realistic and naturally partitioned dataset FEMNIST [2] for evaluation.

Data partitioning strategies. To make a comprehensive analysis, we employ four data partitioning strategies. 1) *Local class-balanced partition*: Each client's dataset maintains strictly equal sample sizes across all classes, ensuring uniform local class distribution. 2) *Pathological partition* [19]: Each client contains data samples from only a small subset of classes (e.g., 1-2 classes), leading to severe distribution skew. Unless otherwise stated, we adopt a single-class-per-client assignment by default to ensure a clear and straightforward comparison of class-wise accuracy. 3) *The Dirichlet partition* [30]: Sample allocation follows a Dirichlet distribution $Dir(\alpha)$ [20] to generate a range of non-i.i.d. data scenarios, enabling comprehensive analysis of the inherent ICD phenomenon and evaluation of the PKD method under varying heterogeneity levels. 4) *FEMNIST's Native Partition*: The dataset's native writer-based partition is preserved to simulate practical FL scenarios. Global class balance across all clients is preserved in all experiments except for FEMNIST, which maintains its natural data distribution.

Models. Similar to [14, 19, 26], LeNet-5 is adopted for the MNIST, FashionMNIST, and FEMNIST datasets by default. We also use the

Table 1: Performance of PKD under the Local Class-Balanced Scenario

#Client	Dataset	MNIST			FashionMNIST			CIFAR-10		
	Method	FedAvg	PKD	Δ	FedAvg	PKD	Δ	FedAvg	PKD	Δ
10	Max.	99.73	99.73	0.00	97.30	97.60	0.30	93.10	93.00	-0.10
	Ave.	99.28	99.32	0.04	89.29	89.50	0.21	83.78	84.93	1.15
	Min.	98.31	98.71	0.40	68.40	76.60	8.20	59.60	71.90	12.30
	Worst	"9"	"9"		"Shirt"	"Shirt"		"Cat"	"Cat"	
100	Max.	99.28	99.29	0.01	96.70	96.60	-0.10	80.90	82.70	1.80
	Ave.	98.11	98.34	0.23	84.66	84.72	0.06	68.52	70.11	1.59
	Min.	96.72	96.92	0.20	51.60	62.30	10.70	46.70	53.00	6.30
	Worst	"9"	"9"		"Shirt"	"Shirt"		"Cat"	"Cat"	

same lightweight network ConvNet-S as in [19] for comparison. (ConvNet-L is simply an extended version of ConvNet-S with an additional 5×5 convolutional layer.) For CIFAR-10 and CIFAR-100, we use ResNet-56 [9] by default and also evaluate with the shallower network VGG-9 [25, 26]. As mentioned in Section 3.1, the expert model adopts the same network structure as the global model, with the exception of the last layer. The number of output neurons is equal to the size of the weak class subset. The number of experts aligns with the number of weak class subsets detailed in Section 2.2: two for MNIST and FashionMNIST, and one for CIFAR-10. Since CIFAR-100 comprises 100 classes, multiple weak class groups exist. We select the G worst-performing groups based on the lowest average accuracy.

Compared Methods. In this section, we compare the performance of the PKD method with the standard baseline, FedAvg, as well as several prior techniques [6, 16, 21, 23, 24] under various data partitioning setups. These advanced techniques include focal loss [16] and data augmentation [6, 24], both designed to mitigate the ICD resulting from class imbalance. We also compare with two other methods, FedProx [23] and FedCofl [21], under the Dirichlet partitions. These methods are designed to alleviate the data heterogeneity problem in FL by either constraining local updates or incorporating global knowledge into the local training process through KD. Our analysis reveals that while current approaches effectively alleviate general data heterogeneity, they remain insufficient in addressing the inherent ICD problem.

Hyperparameters. Stochastic Gradient Descent (SGD) is employed for optimization, with a learning rate of 0.01. Same as FedAvg [19], the number of local epochs and the batch size are set to 5 and 50, respectively. The networks are trained for 100 rounds on MNIST and up to 300 rounds on other datasets. The total number of clients is set to 10 by default. We also scale this default value to 100 across various benchmarks and vary the fraction of clients selected at each round to evaluate PKD under different setups. Three fractions are used on the FEMNIST dataset, including 0.1, 0.5, and 1.0. During the PKD process, the hyperparameter T is set to 5. The value of λ is set to 1.0 for MNIST, FashionMNIST, and FEMNIST, and to 0.5 for CIFAR-10 and CIFAR-100.

Implementation. All experiments are implemented in Python using the PyTorch framework. Training is conducted on a server running Ubuntu, equipped with 4 NVIDIA RTX 3090 GPUs, 2 Intel Xeon Platinum 8269CY CPUs, and 128 GB of RAM.

Table 2: Results for Other Neural Networks under the Local Class-Balanced Scenario

Dataset	FashionMNIST			CIFAR-10		
	ConvNet-S			VGG-9		
Method	FedAvg	PKD	Δ	FedAvg	PKD	Δ
Max.	98.20	98.20	0.00	92.50	92.60	0.10
Ave.	90.43	90.92	0.49	83.04	83.48	0.44
Min.	70.50	75.30	4.80	65.10	72.30	7.20
Worst	"Shirt"	"Shirt"		"Cat"	"Cat"	

Table 3: Performance of PKD under the Pathological Data Partition Scenario

Dataset	MNIST			FashionMNIST			CIFAR-10		
	1			1			2		
Method	FedAvg	PKD	Δ	FedAvg	PKD	Δ	FedAvg	PKD	Δ
Max.	96.02	99.03	3.01	91.20	91.40	0.20	72.10	80.30	8.20
Ave.	75.85	84.45	8.60	47.39	71.03	23.64	38.64	41.42	2.78
Min.	7.90	68.38	60.48	0.00	51.80	51.80	2.90	16.10	13.20
Worst	"8"	"9"		"Shirt"	"Shirt"		"Bird"	"Cat"	

4.2 Performance of the Proposed Method

Table 1 presents the performance of our proposed method under *local class-balanced scenario* as described in Section 4.1. In the baseline scenario with 10 clients, the inter-class accuracy discrepancy is 1.42%, 28.9% and 33.5% for MNIST, FashionMNIST and CIFAR-10, respectively. The proposed PKD method can improve the accuracy of the worst-performing classes by 0.4%, 8.2% and 12.3%, respectively, without comprising the global average accuracy. The overall model performance degrades as the number of clients increases to 100. In this case, PKD can improve the worst class-wise accuracy by 0.2%, 10.7%, and 6.3% on MNIST, FashionMNIST, and CIFAR-10, respectively. It is worth noting that improving the accuracy of weak classes usually does not compromise the model performance on other classes. The accuracy of dominant classes remains largely unchanged or is even slightly improved. As a result, the global average accuracy also increases. As mentioned in Section 4.1, we employ LeNet-5 as the baseline architecture for evaluations on MNIST and FashionMNIST, while utilizing ResNet-56 for CIFAR-10. For a comprehensive comparison, Table 2 further presents the performance of PKD for additional network architectures.

Table 3 shows the performance of PKD under the *pathological partition scenario*. The number of classes per client (#Class/Client) is set to 1 for MNIST and FashionMNIST, and to 2 for CIFAR-10. Similar to the results reported in [15], the global accuracy becomes low under such an extremely unbalanced distribution. Compared to local class-balanced scenarios, performance improvements for the worst-performing classes are more pronounced, as shown in Table 3. The minimum class-wise accuracy increases by 60.5% on MNIST, 51.8% on FashionMNIST, and 13.2% on CIFAR-10, respectively. As a result, the global average accuracy is also improved. As shown in Fig. 9, the accuracy of weak classes becomes significantly more stable compared to the baseline case.

Table 4 presents the experimental results under the *Dirichlet partition scenario*. The concentration parameter α in $Dir(\alpha)$ is set to

Table 4: Performance of PKD under the Dirichlet Partition Scenario (*Dir* (0.5))

Dataset	MNIST			FashionMNIST			CIFAR-10		
Method	FedAvg	PKD	Δ	FedAvg	PKD	Δ	FedAvg	PKD	Δ
Max.	99.64	99.64	0.00	96.90	96.90	0.00	92.90	93.80	0.90
Ave.	98.72	98.84	0.12	86.05	86.20	0.15	76.38	77.92	1.54
Min.	96.63	97.02	0.39	53.10	63.20	10.10	55.30	61.40	6.10
Worst	"9"	"9"		"Shirt"	"Shirt"		"Dog"	"Cat"	


Figure 9: Accuracy of the Worst-performing Class ‘Shirt’ during Training. (FashionMNIST, #Class/Client=1)

0.5. The overall model performance is better than in the pathological partition scenario. However, the baseline methods still exhibit 3.01% inherent ICD on MNIST, 43.8% on FashionMNIST, and 37.6% on CIFAR-10. Our PKD approach improves the minimum class-wise accuracy by 0.39%, 10.10%, and 6.10%, respectively, without affecting the average accuracy.

Table 5 presents the results on the FEMNIST dataset based on its native partition. The dataset comprises of over 3000 users and 62 classes, including digits, uppercase, and lowercase letters. To make a direct comparison with the MNIST dataset, we retain only the digit samples and their corresponding users. In realistic FL scenarios, not all users participate in every communication round. To simulate this, we set the fraction of clients selected at each round to 0.1, 0.5, and 1.0, respectively. This participation fraction applies to both the expert learning and the global model learning processes. PKD shows consistent improvements across different fractions, increasing the minimum class-wise accuracy by 1.4%, 1.5%, and 1.7%, respectively.

4.3 Comparison with Existing Techniques

Table 6 compares the proposed method with several existing techniques that tackle the ICD problem induced by class imbalance. An effective approach to address the class imbalance issue is to offset the negative impact brought by the uneven class distribution [5, 16]. It can be done by either re-sampling the minority classes or assigning larger weights to their loss values while calculating the empirical risk. Here we adopt a similar idea as [16] and test its performance for alleviating the inherent ICD problem. Instead of up-weighting the minority classes, we dynamically enhance the weights of the inherent weak classes when calculating the loss value. The result indicates that directly applying this method may not alleviate the inherent ICD problem. It is observed that the minimum class-wise accuracy drops due to increased disparity among weak classes within a group. Take the weak class group {‘shirt’, ‘coat’, ‘pullover’} in Fig. 6 as an example. As mentioned in Section 2.2, an improvement in the accuracy of one weak class is generally accompanied by a corresponding decrease in the accuracy of other weak

Table 5: Experimental Results on the FEMNIST Dataset

Dataset	FEMNIST								
Fraction	0.1			0.5			1.0		
Method	FedAvg	PKD	Δ	FedAvg	PKD	Δ	FedAvg	PKD	Δ
Max.	98.10	98.10	0.00	98.10	98.20	0.10	98.10	98.20	0.10
Ave.	92.30	92.56	0.26	92.78	93.00	0.22	92.96	93.27	0.31
Min.	87.50	89.20	1.70	88.20	89.70	1.50	88.60	90.00	1.40

Table 6: Comparison with Existing ICD Solutions for the Class Imbalance Problem.

Setup	FashionMNIST, Local Class Balance, #client=10									
Method	Fedavg	Re-weighting			Data Augmentation				Ours	
		Focal loss			Sample-level		Feature-level			
		[19]	[16]	Δ	[6]	Δ	[24]	Δ		
Max.	97.30	97.80	0.50	97.40	0.10	97.40	0.10	97.60	0.30	
Ave.	89.29	88.64	-0.65	85.04	-4.25	89.52	0.23	89.50	0.21	
Min.	68.40	65.40	-3.00	53.80	-14.60	70.70	2.30	76.60	8.20	

classes. Suppose at a given epoch, ‘pullover’ is the worst-performing class and assigned a large weight while calculating the total loss. In subsequent iterations, the model is updated to focus more on improving performance for ‘pullover’. However, this improvement may come at the cost of degraded performance on the other two weak classes, thereby resulting in no significant improvement in overall accuracy. In [6] and [24], data augmentation is applied at the sample level and feature level, respectively, to implicitly enhance data diversity. These two approaches are commonly used to improve the model’s performance on minority classes. The results suggest that feature-level data augmentation can modestly mitigate the inherent ICD issue, leading to a 2.30% improvement in the accuracy of the worst-performing class.

Table 7 compares the proposed method with FedProx [23] and FedCodl [21] under the Dirichlet partition scenario. These methods are designed to tackle data heterogeneity in FL. Specifically, FedProx introduces a proximal term to the objective to constrain local updates and uses a hyperparameter μ to control its strength. FedCodl, on the other hand, adopts a KD framework, encouraging local models to align with the global model by minimizing the KL divergence between their output logits. Experimental results show that while existing methods can mitigate general data heterogeneity and improve overall model performance, they exhibit limited effectiveness in enhancing accuracy for weak classes compared to the proposed approach.

4.4 Performance on More Complex Datasets

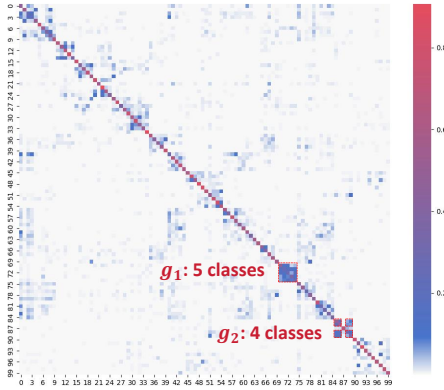
To assess the effectiveness of this approach on more complex datasets with higher class diversity, we further evaluate its performance on CIFAR-100, which comprises 100 classes. We maintain a local class-balanced partition across 10 clients and compare PKD to the baseline. Similar to Fig. 4(c) for FashionMNIST, Fig. 10 maps the predictions to their respective original classes. Given that CIFAR-100 has a large number of classes, the weak class groups are expected to increase in size. For the PKD implementation, we select G groups

Table 7: Comparison with Existing Data-Heterogeneity Solutions

Setup		FashionMNIST, Dir(0.5), #client=20									
Method	Fedavg [19]	FedProx[23]				FedCodi		Ours			
		$\mu = 0.001$	Δ	$\mu = 0.002$	Δ	[21]	Δ	PKD	Δ		
Max.	96.90	97.00	0.10	97.30	0.40	97.50	0.60	96.90	0.00		
Ave.	86.05	86.17	0.12	86.06	0.01	86.59	0.54	86.20	0.15		
Min.	53.10	56.90	3.80	55.60	2.50	53.80	0.70	63.20	10.10		

Table 8: Experimental Results on the CIFAR-100 Dataset.

Setup		CIFAR-100, Local Class Balance, #client=10			
Method	FedAvg	PKD			
		$G = 1$	Δ	$G = 2$	Δ
Max.	91.00	92.00	1.00	92.00	1.00
Ave.	62.82	64.02	1.20	62.91	0.09
Min.	27.00	30.00	3.00	32.00	5.00

**Figure 10: Prediction Results of ResNet-56 on CIFAR-100.**

with the poorest average accuracy. Due to constraints on the number of experts and corresponding overhead, G is set to a small value, specifically 1 or 2, in line with other datasets. The number of weak classes in the two groups is 5 and 4, respectively. The results are shown in Table 8. Despite utilizing only 1-2 expert models, the PKD method achieves a 3-5% improvement in minimum class-wise accuracy.

4.5 Overhead Analysis

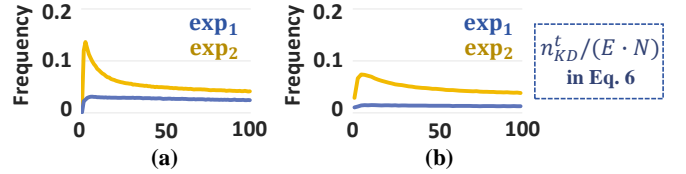
In the proposed PKD method, the computational overhead mainly comes from expert training at Stage 2 and the computation of soft labels (p_e) during Stage 3. As shown in Eq. 5, the computation cost of expert training is proportional to the total sample size of the weak classes ($\sum_i n_{g_i}$). The actual computation cost for expert training ranges from $2.1U$ to $40U$ under different setups, where U is the computation load of a local training round in the baseline scenario (FedAvg), as described in Eq. 3. For Stage 3, the computational overhead primarily depends on the value of $\frac{n_{KD}^t}{E \cdot N}$ in Eq. 6. Fig. 11 shows the frequency with which an expert is activated for KD. The value

Table 9: Computation Cost in the Local Class-Balanced Scenario (Unit: U , which is 374.87 GFLOPs for the Benchmark)

Setup		FashionMNIST, Local Class Balance, #client=10									
Method		Target Min. Acc.					Final Acc.				
		40%	50%	60%	65%	70%	Min.	Ave.			
FedAvg [19]	13	19	30	57	-	-	68.4%	89.3%			
Focal Loss [16]	14	23	56	72	-	-	65.4%	88.6%			
Data Aug. [6]	29	67	-	-	-	-	53.8%	85.0%			
Data Aug. [24]	14	20	37	63	87	-	70.7%	89.5%			
PKD	44.1	50.4	53.5	55.5	76.1	-	76.6%	89.5%			

Table 10: Computation Cost in the Dirichlet Partition Scenario (Unit: Same as Table 9)

Setup		FashionMNIST, Dir(0.5), #client=20									
Method		Target Min. Acc.					Final Acc.				
		30%	45%	50%	55%	60%	Min.	Ave.			
FedAvg [19]	16	27	41	-	-	-	53.1%	86.0%			
FedProx [23]	18	25	36	48	-	-	56.9%	86.2%			
FedCodi [21]	20	28	35	46	-	-	55.1%	86.6%			
PKD	25.2	30.4	35.5	43.6	58.9	-	63.2%	86.2%			

**Figure 11: Expert Activation Frequency for FashionMNIST under (a) the Local Class-Balanced Scenario and (b) the Dirichlet Partition $Dir(0.5)$ Scenario.**

of $\frac{n_{KD}^t}{E \cdot N}$ increases rapidly at the onset of training and then gradually decreases as training progresses. KD occurs less frequently because, as the performance of the student model improves during training, fewer samples from the weak classes are misclassified. Since PKD is applied only under specific conditions, the computational overhead for Stage 3 remains below $0.2U$ per round across all benchmarks and setups in this work.

Table 9 reports the computation cost (measured in U) required to achieve the target minimum class-wise accuracy under the local class-balanced scenario. The symbol ‘-’ indicates a failure to reach the target accuracy. The reported results for PKD reflect the total amount of computations across all three stages. Before the PKD stage, the model undergoes 20 rounds of warmup and 25 rounds of expert learning. The combined computational cost for these two phases is $32.5U$. As a result, the overall computational overhead of PKD is relatively high initially, particularly when the minimum accuracy is below 50%. Nonetheless, the model converges more rapidly than the baseline, requiring fewer computations to achieve the same level of accuracy in later training stages. A similar trend has been observed under other setups. The computation cost in

the Dirichlet partition scenario is shown in Table 10. For FedCodl, we assume that the soft labels are precomputed and reused across multiple local epochs, and the inference cost of the teacher model is ignored. Besides, the computation cost for the proximal term in FedProx is also ignored for simplicity.

5 Conclusion

In this work, we investigate an interesting phenomenon that weak classes consistently exist even for class-balanced learning. A class-specific partial knowledge distillation method is proposed to mitigate this inherent inter-class discrepancy.

References

- [1] Mateusz Buda, Atsuto Maki, and Maciej A. Mazurowski. 2018. A systematic study of the class imbalance problem in convolutional neural networks. *Neural Networks* 106 (2018), 249–259. doi:10.1016/j.neunet.2018.07.011
- [2] Sebastian Caldas, Peter Wu, Tian Li, Jakub Konečný, H. Brendan McMahan, Virginia Smith, and Ameet Talwalkar. 2018. LEAF: A Benchmark for Federated Settings. *CoRR abs/1812.01097* (2018). arXiv:1812.01097
- [3] Nitesh V. Chawla, Kevin W. Bowyer, Lawrence O. Hall, and W. Philip Kegelmeyer. 2002. SMOTE: Synthetic Minority Over-sampling Technique. *J. Artif. Intell. Res.* 16 (2002), 321–357. doi:10.1613/JAIR.953
- [4] Jiequan Cui, Shu Liu, Zhuotao Tian, Zhisheng Zhong, and Jiaya Jia. 2023. ResLT: Residual Learning for Long-Tailed Recognition. *IEEE Transactions on Pattern Analysis and Machine Intelligence* 45, 3 (2023), 3695–3706. doi:10.1109/TPAMI.2022.3174892
- [5] Yin Cui, Menglin Jia, Tsung-Yi Lin, Yang Song, and Serge J. Belongie. 2019. Class-Balanced Loss Based on Effective Number of Samples. In *IEEE Conference on Computer Vision and Pattern Recognition, CVPR 2019, Long Beach, CA, USA, June 16–20, 2019*. Computer Vision Foundation / IEEE, 9268–9277. doi:10.1109/CVPR.2019.00949
- [6] Terrance Devries and Graham W. Taylor. 2017. Improved Regularization of Convolutional Neural Networks with Cutout. *CoRR abs/1708.04552* (2017). arXiv:1708.04552 <http://arxiv.org/abs/1708.04552>
- [7] Andrew Estabrooks, Taeho Jo, and Nathalie Japkowicz. 2004. A Multiple Resampling Method for Learning from Imbalanced Data Sets. *Comput. Intell.* 20, 1 (2004), 18–36. doi:10.1111/J.0824-7935.2004.T01-1-00228.X
- [8] Haibo He and Edward A. Garcia. 2009. Learning from Imbalanced Data. *IEEE Transactions on Knowledge and Data Engineering* 21, 9 (2009), 1263–1284. doi:10.1109/TKDE.2008.239
- [9] Kaiming He, Xiangyu Zhang, Shaoqing Ren, and Jian Sun. 2016. Deep Residual Learning for Image Recognition. In *2016 IEEE Conference on Computer Vision and Pattern Recognition (CVPR)*, 770–778. doi:10.1109/CVPR.2016.90
- [10] Geoffrey Hinton, Oriol Vinyals, and Jeff Dean. 2015. Distilling the Knowledge in a Neural Network. arXiv:1503.02531 [stat.ML] <https://arxiv.org/abs/1503.02531>
- [11] Jaehyung Kim, Jongheon Jeong, and Jinwoo Shin. 2020. M2m: Imbalanced Classification via Major-to-Minor Translation. In *2020 IEEE/CVF Conference on Computer Vision and Pattern Recognition, CVPR 2020, Seattle, WA, USA, June 13–19, 2020*. Computer Vision Foundation / IEEE, 13893–13902. doi:10.1109/CVPR42600.2020.01391
- [12] Alex Krizhevsky. 2009. *Learning multiple layers of features from tiny images*. Technical Report. Univ. of Toronto, Toronto, Canada.
- [13] Y. Lecun, L. Bottou, Y. Bengio, and P. Haffner. 1998. Gradient-based learning applied to document recognition. *Proc. IEEE* 86, 11 (1998), 2278–2324. doi:10.1109/5.726791
- [14] Zexi Li, Tao Lin, Xinyi Shang, and Chao Wu. 2023. Revisiting weighted aggregation in federated learning with neural networks. In *Proceedings of the 40th International Conference on Machine Learning (Honolulu, Hawaii, USA) (ICML’23)*. JMLR.org, Article 816, 22 pages.
- [15] Zijian Li, Jiawei Shao, Yuyi Mao, Jessie Hui Wang, and Jun Zhang. 2022. Federated learning with gan-based data synthesis for non-iid clients. In *International workshop on trustworthy federated learning*. Springer, 17–32.
- [16] Tsung-Yi Lin, Priya Goyal, Ross B. Girshick, Kaiming He, and Piotr Dollár. 2020. Focal Loss for Dense Object Detection. *IEEE Trans. Pattern Anal. Mach. Intell.* 42, 2 (2020), 318–327. doi:10.1109/TPAMI.2018.2858826
- [17] Bo Liu, Haoxiang Li, Hao Kang, Gang Hua, and Nuno Vasconcelos. 2022. Bread-crumbs: Adversarial Class-Balanced Sampling for Long-Tailed Recognition. In *Computer Vision – ECCV 2022*, Shai Avidan, Gabriel Brostow, Moustapha Cissé, Giovanni Maria Farinella, and Tal Hassner (Eds.). Springer Nature Switzerland, Cham, 637–653.
- [18] Jialun Liu, Yifan Sun, Chuchu Han, Zhaopeng Dou, and Wenhui Li. 2020. Deep Representation Learning on Long-Tailed Data: A Learnable Embedding Augmentation Perspective. In *2020 IEEE/CVF Conference on Computer Vision and Pattern Recognition, CVPR 2020, Seattle, WA, USA, June 13–19, 2020*. Computer Vision Foundation / IEEE, 2967–2976. doi:10.1109/CVPR42600.2020.00304
- [19] Brendan McMahan, Eider Moore, Daniel Ramage, Seth Hampson, and Blaise Agüera y Arcas. 2017. Communication-Efficient Learning of Deep Networks from Decentralized Data. In *Proceedings of the 20th International Conference on Artificial Intelligence and Statistics (Proceedings of Machine Learning Research, Vol. 54)*, Aarti Singh and Jerry Zhu (Eds.). PMLR, 1273–1282. <https://proceedings.mlr.press/v54/mcmahan17a.html>
- [20] Thomas Minka. 2000. Estimating a Dirichlet distribution.
- [21] Xuanming Ni, Xinyuan Shen, and Huimin Zhao. 2022. Federated optimization via knowledge codistillation. *Expert Systems with Applications* 191 (2022), 116310. doi:10.1016/j.eswa.2021.116310
- [22] Jiawei Ren, Cunjun Yu, shunan sheng, Xiao Ma, Haiyu Zhao, Shuai Yi, and hongsheng Li. 2020. Balanced Meta-Softmax for Long-Tailed Visual Recognition. In *Advances in Neural Information Processing Systems*, H. Larochelle, M. Ranzato, R. Hadsell, M.F. Balcan, and H. Lin (Eds.), Vol. 33. Curran Associates, Inc., 4175–4186.
- [23] Anit Kumar Sahu, Tian Li, Maziar Sanjabi, Manzil Zaheer, Ameet Talwalkar, and Virginia Smith. 2018. On the Convergence of Federated Optimization in Heterogeneous Networks. *CoRR abs/1812.06127* (2018). arXiv:1812.06127
- [24] Xian Shuai, Yulin Shen, Siyang Jiang, Zhihe Zhao, Zhenyu Yan, and Guoliang Xing. 2022. BalanceFL: Addressing Class Imbalance in Long-Tail Federated Learning. In *21st ACM/IEEE International Conference on Information Processing in Sensor Networks, IPSN 2022, Milano, Italy, May 4–6, 2022*. IEEE, 271–284. doi:10.1109/IPSNS4338.2022.00029
- [25] Karen Simonyan and Andrew Zisserman. 2014. Very deep convolutional networks for large-scale image recognition. *arXiv preprint arXiv:1409.1556* (2014).
- [26] Hongyi Wang, Mikhail Yurochkin, Yuekai Sun, Dimitris Papailiopoulos, and Yasaman Khazaeni. 2020. Federated Learning with Matched Averaging. arXiv:2002.06440 [cs.LG] <https://arxiv.org/abs/2002.06440>
- [27] Liuyu Xiang, Guiguang Ding, and Jungong Han. 2020. Learning From Multiple Experts: Self-paced Knowledge Distillation for Long-Tailed Classification. In *Computer Vision – ECCV 2020 - 16th European Conference, Glasgow, UK, August 23–28, 2020, Proceedings, Part V (Lecture Notes in Computer Science, Vol. 12350)*, Andrea Vedaldi, Horst Bischof, Thomas Brox, and Jan-Michael Frahm (Eds.). Springer, 247–263. doi:10.1007/978-3-030-58558-7_15
- [28] Han Xiao, Kashif Rasul, and Roland Vollgraf. 2017. Fashion-MNIST: a Novel Image Dataset for Benchmarking Machine Learning Algorithms. *CoRR abs/1708.07747* (2017). arXiv:1708.07747
- [29] Dezhong Yao, Wanning Pan, Yutong Dai, Yao Wan, Xiaofeng Ding, Chen Yu, Hai Jin, Zheng Xu, and Lichao Sun. 2023. FedGKD: Toward heterogeneous federated learning via global knowledge distillation. *IEEE Trans. Comput.* 73, 1 (2023), 3–17.
- [30] Mikhail Yurochkin, Mayank Agarwal, Soumya Ghosh, Kristjan Greenewald, Nghia Hoang, and Yasaman Khazaeni. 2019. Bayesian nonparametric federated learning of neural networks. In *International conference on machine learning*. PMLR, 7252–7261.
- [31] Jing Zhang, Chuanwen Li, Jianzong Qi, and Jiayuan He. 2023. A Survey on Class Imbalance in Federated Learning. arXiv:2303.11673 [cs.LG] <https://arxiv.org/abs/2303.11673>
- [32] Yifan Zhang, Bingyi Kang, Bryan Hooi, Shuicheng Yan, and Jiashi Feng. 2023. Deep Long-Tailed Learning: A Survey. *IEEE Trans. Pattern Anal. Mach. Intell.* 45, 9 (2023), 10795–10816. doi:10.1109/TPAMI.2023.3268118
- [33] Fengpan Zhao, Yan Huang, Akshita Maradapu Vera Venkata Sai, and Yubao Wu. 2020. A Cluster-based Solution to Achieve Fairness in Federated Learning. In *2020 IEEE Intl Conf on Parallel & Distributed Processing with Applications, Big Data & Cloud Computing, Sustainable Computing & Communications, Social Computing & Networking (ISPA/BDCloud/SocialCom/SustainCom)*, 875–882. doi:10.1109/ISPA-BDCloud-SocialCom-SustainCom51426.2020.00135